Author/s:
Adamson, BD;Coughlan, NJA;Markworth, PB;Continetti, RE;Bieske, EJ

Title:
An ion mobility mass spectrometer for investigating photoisomerization and photodissociation of molecular ions

Date:
2014-12-01

Citation:
Adamson, B. D., Coughlan, N. J. A., Markworth, P. B., Continetti, R. E. & Bieske, E. J. (2014). An ion mobility mass spectrometer for investigating photoisomerization and photodissociation of molecular ions. Review of Scientific Instruments, 85 (12), https://doi.org/10.1063/1.4903753.

Persistent Link:
https://hdl.handle.net/11343/52029

An Ion Mobility Mass Spectrometer for Investigating Photoisomerization and Photodissociation of Molecular Ions

B. D. Adamson,[1] N. J. A. Coughlan,[1] P. B. Markworth,[1] R.E. Continetti,[2] and E. J. Bieske[1, a)]

[1)] *School of Chemistry, The University of Melbourne, Victoria,
Australia 3010*

[2)] *Department of Chemistry and Biochemistry, University of California, San Diego,
9500 Gilman Drive, La Jolla, CA 92093-0340*

(Dated: 13 November 2014)

An ion mobility mass spectrometry apparatus for investigating the photoisomerization and photodissociation of electrosprayed molecular ions in the gas phase is described. The device consists of a drift tube mobility spectrometer, with access for a laser beam that intercepts the drifting ion packet either coaxially or transversely, followed by a quadrupole mass filter. An ion gate halfway along the drift region allows the instrument to be used as a tandem ion mobility spectrometer, enabling mobility selection of ions prior to irradiation, with the photoisomer ions being separated over the second half of the drift tube. The utility of the device is illustrated with photoisomerization and photodissociation action spectra of carbocyanine molecular cations. The mobility resolution of the device for singly charged ions is typically 80 and it has a mass range of 100-440 Da, with the lower limit determined by the drive frequency for the ion funnels, and the upper limit by the quadrupole mass filter.

Keywords: ion mobility spectrometry, photoisomerization, ion spectroscopy, mass spectrometry

---

[a)] corresponding author: evanjb@unimelb.edu.au

I. INTRODUCTION

Molecular isomerization plays a key role in many natural and man-made photochemical processes. For example, the retinal protonated Schiff base is the key photoactive unit in the visual transduction cycle and in bacterial photosynthesis, where in both cases its action involves isomerization about C=C bonds along the polyene chain. Chemists and material scientists are currently attempting to harness photoisomerizing molecules such as azobenzenes, diarylethenes and spiropyrans as light-activated engines in molecular machines.[1–3] In order to understand and model photoactive systems there are significant advantages in examining the core molecules in the gas phase, due to the relative ease with which gas-phase data can be compared with accurate calculations for isolated molecules. Here we describe an instrument for probing the photoisomerization of biologically and technologically important molecular ions in the gas phase based on photo-induced changes in the molecules' drift velocity as they pass through a gas cell. The technique's foundation is ion mobility mass spectrometry (IMMS), a method whereby charged molecules are separated on the basis of both mass and shape. Typically, a packet of molecular ions, formed through either electrospray ionization or laser desorption, is propelled by an electric field through a drift tube containing a buffer gas (normally He or N_2). Extended or uncoiled molecules tend to travel more slowly through the buffer gas than folded, compact molecules, allowing spatial and temporal separation of a structurally heterogeneous population of molecular ions into packets of its constituent isomers. The ions pass from the drift tube into a mass spectrometer in order to measure their mass distribution. IMMS has been used to examine isomers for an enormous range of molecules including peptides, proteins, carbohydrates, and clusters.[4–11]

The IMMS apparatus described in this paper has been developed to accommodate laser excitation of drifting charged molecules in order to probe their photoisomerization behaviour. Previously, the transformation from one configurational isomer to another in IMMS devices has been promoted using collisional heating in a short section of the drift region,[12] or by heating the gas in the drift region.[13,14] Laser excitation provides a potentially more selective means for activating molecular ions, with control over both excitation wavelength and beam intensity. Molecular ions typically have electronic transitions in the visible or ultraviolet range, permitting straightforward energisation using photoexcitation.

For many molecules, rapid non-radiative deactivation (internal conversion, intersystem crossing) transforms electronic energy into vibrational energy allowing isomerization barriers to be overcome, leading to changes in molecular geometry and collision cross section. Alternatively, for some molecules photoisomerization can be initiated through dynamics on the excited state potential energy surface (PES), proceeding through a conical intersection to the isomer region of the ground state PES.[15]

Significantly, by measuring the photo-isomer yield as a function of laser wavelength one can derive an action spectrum that represents the molecule's absorption spectrum $A(\lambda)$ convoluted with a wavelength-dependent isomerization yield $\phi(\lambda)$. If $\phi(\lambda)$ is independent of λ, the photoisomerization action spectrum mimics the absorption spectrum. This form of photoisomerization action (PISA) spectroscopy complements existing spectroscopic techniques for probing molecular ions, including resonance enhanced photodissociation,[16–18] zero kinetic energy (ZEKE) photoelectron spectroscopy,[19] mass analysed threshold ionisation (MATI) spectroscopy,[20] and laser induced fluorescence (LIF).[21] The approach described in this paper differs from previous methods because the detectable "action" is a change in ion drift speed, rather than photodissociation, photoelectron ejection, or photon emission. An important advantage of our machine is that it is possible to measure PISA spectra for mobility-selected isomers. Previously isomer specific spectra for molecular ions have been measured using IR-UV double resonance REPD, or by REPD with preselection of the ions using field asymmetric ion mobility spectrometry (FAIMS).[22]

The new IMMS machine has been employed to investigate photoisomerization of molecules containing conjugated carbon chains including carbocyanine dyes HITC$^+$ and DTC$^+$,[23,24] and the retinal protonated Schiff base.[25] The apparatus has also been used to structurally characterise charged fragments from retinal protonated Schiff base, helping to unravel the photodissociation mechanism.[26] In this paper we provide a comprehensive description of the apparatus, illustrating its capacity to characterize photoisomerization and photofragmentation processes using the positively charged carbocyanine dye molecules DTC$^+$and DCY4$^+$ as examples.

II. BACKGROUND

In its simplest form, ion mobility mass spectrometry involves injecting a packet of ions into a drift cell filled with buffer gas where they are subject to an electric field. For low electric fields the ions' drift velocity v_d is proportional to the electric field E and is given by,[27]

$$v_d = K \times E \tag{1}$$

where K is the ion mobility. The mobility is in turn related to the collision integral, $\Omega^{(1,1)}(T)$, through the Mason-Schamp equation,[27,28]

$$K = \frac{3ze}{16N} \left(\frac{2\pi}{\mu k_B T} \right)^{1/2} \frac{1}{\Omega^{(1,1)}(T)}. \tag{2}$$

In Eqn. 2, z is the number of elementary charges on the ion, e is the electronic charge, N is the number density of buffer gas molecules, k_B is the Boltzmann constant, and $\mu = Mm/(M+m)$ is the reduced mass (m and M are the masses of the drifting ion and buffer gas molecule, respectively). The collision integral, $\Omega^{(1,1)}(T)$, which for hard spheres is the collision cross section, is related to the deflection angle of the collision partners averaged over impact parameter, collision orientation and velocity. Because $\Omega^{(1,1)}(T)$ depends on the intermolecular potential energy surface (PES) describing the interaction of the molecular ion and the buffer gas atom, it is sensitive to the molecular conformation and therefore changes following photoisomerization.

The drift region is normally operated in the low field regime such that the mobility is independent of field strength and the field-induced collision energy is much less than the thermal energy. The regime is defined by the relationship,[27]

$$\frac{Mv_d^2}{3kT} << 1 \tag{3}$$

Under these conditions the effective temperature of the drifting ions is close to that of the buffer gas (300 K). The collision rate for the molecular ions drifting in He or N_2 at 10 Torr, estimated from the Langevin rate, is $\approx 3 \times 10^8\, s^{-1}$.

To establish contact between the measured ion mobility (K) and the molecular structure, the mobility is normally predicted using the MOBCAL program developed by Jarrold and coworkers.[29–31] Three methods are commonly used. First, the simple projection approximation (PA) assumes hard sphere collisions and averages the projected cross section over collision orientations. Second, the exact hard sphere scattering (EHSS) method is similar to the PA method but accounts for multiple scattering collisions, important for molecules with convexities. Third, the trajectory method (TM) uses classical trajectory simulations to determine the average momentum transfer occurring from interactions between the molecular ion and a neutral gas molecule, with the intermolecular interaction represented as the sum of atom-atom Lennard-Jones interaction terms supplemented by charge-induced dipole induction terms. The necessary isomer geometries for the mobility calculations are obtained using *ab initio* or density functional theory (DFT) calculations.

III. INSTRUMENT CONSTRUCTION

A. Overview

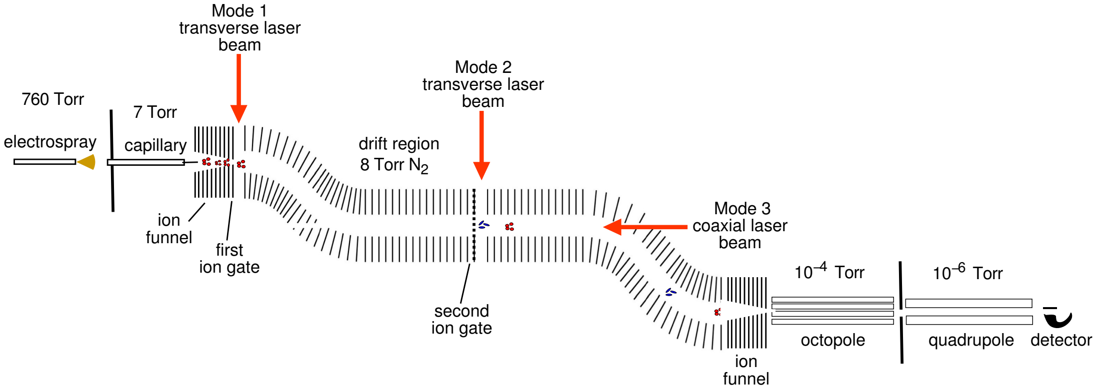

FIG. 1. Schematic view of the ion mobility mass spectrometer. Ions from an electrospray ion source pass through a heated desolvation capillary, and into an ion funnel (IF1). Ions are injected from IF1 through an ion gate into the drift region filled with N_2 gas ($P \approx 8$ torr) and subjected to an electric field of ≈40 V/cm. After passing through the drift tube, ions are collected by a second ion funnel, travel through an octopole ion guide, are mass selected by a quadrupole mass filter, and sensed by an ion detector. Ions can be irradiated by a transverse laser beam after the firstion gate (**Mode 1**), by a transverse laser beam halfway along the drift region after the second ion gate (**Mode 2**), or coaxially in the middle section of the drift region (**Mode 3**).

The machine is essentially a conventional ion mobility spectrometer with provision for a laser beam to overlap the drifting ions coaxially or transversely. As shown in Fig. 1, electrosprayed ions pass through a heated transfer capillary and accumulate in the first

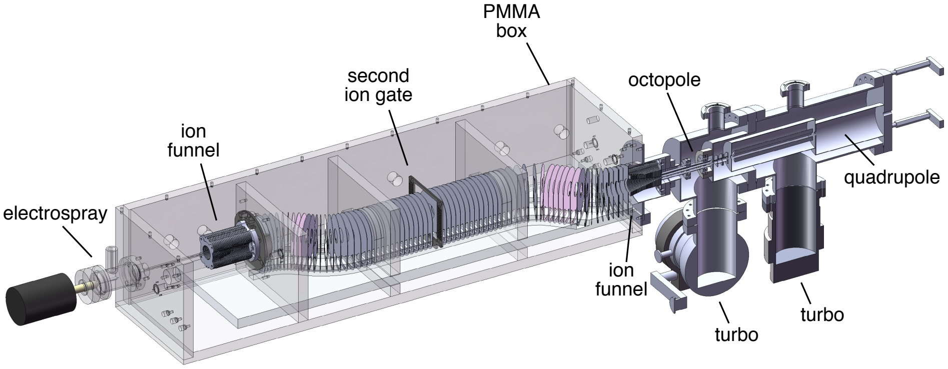

FIG. 2. A section of the IMMS apparatus, showing electrospray ion source, first ion funnel, second ion gate, second ion funnel, octopole ion guide, quadrupole mass filter.

ion funnel. An electrostatic ion gate periodically injects ion bunches into the drift section filled with low pressure N_2 or He gas (P=5-15 Torr) where the ions are subjected to a drift field of $\approx$40 V/cm. Following the drift region the ions are collected by a second ion funnel, before passing through a small orifice, an octopole ion guide, quadrupole mass filter, and finally being sensed by an ion detector. The ions can either be irradiated by a transverse laser beam immediately after the first ion gate or halfway through the drift region after a second ion gate (used to mobility-select bunches of ions), or coaxially in the middle section of the drift region. These different excitation modes are described below (Section III I). Irrespective of where photoexcitation occurs, a photo-induced change in ion conformation and drift mobility results in spatial and temporal separation of the photo-isomer ions from the parent ions over the remaining section of the drift region.

B. Housing

The first ion funnel, drift region and second ion funnel are contained in a purpose-built poly(methyl methacrylate) (PMMA) box, with internal dimensions $l = 1130\,\mathrm{mm}$, $w = 350\,\mathrm{mm}$, $h = 220\,\mathrm{mm}$ (wall thickness 25 mm) and a removable lid sealed by an O-ring. Three interior PMMA baffles support the box, reducing mechanical deformation when it is pumped down to normal operating pressure (5-15 Torr). The octopole ion guide and quadrupole mass filter are housed in a tubular stainless steel chamber (150 mm diameter) divided into two differentially pumped chambers, and which has ports for connecting turbo molecular pumps, electrical feedthroughs, and vacuum gauges.

C. Gas Flow and Pumping

The drift region is pumped by a 28 m^3/hr dual-vane rotary pump (Edwards E2M28), connected via a foreline trap to the source side of the first ion funnel. Buffer gas (either He or N_2) is supplied to the chamber towards the exit end via a mass flow controller (Sevenstar D08-1F). The flow rate is normally 0.2 SLM. This results in a counterflow of buffer gas back through the first ion funnel, preventing neutral molecules (particularly solvent vapour from the electrospray) entering the drift region. The pressure in the drift chamber is controlled by a combination of adjusting the buffer gas flow rate and choking the outlet flow with a valve. The octopole chamber is pumped by a 330 L/s turbo molecular pump and typically has a pressure of 10^{-3} Torr, while the quadrupole chamber is evacuated by a 230 L/s turbo molecular pump and has an operational pressure of $\leq 4\times10^{-6}$ Torr.

D. Electrospray Ion Source

The ion source is a homebuilt electrospray unit. Typically, the analyte is dissolved in either acetonitrile or 50:50 methanol:water and delivered at 5-20 μL/min using a syringe pump to a stainless steel capillary. The capillary tip is positioned 3-6 mm from the desolvation capillary entrance, and at a potential of 3-5 kV relative to the desolvation capillary. The electrospray assembly is contained in a glass tube (50 mm diameter), filled with flowing N_2 gas at atmospheric pressure. The ions enter a stainless steel desolvation capillary (ID 0.8 mm) sealed within a glass tube that passes into the PMMA box through a 1/4″ Cajon fitting. Inside the PMMA box, the desolvation capillary is wrapped with nichrome wire carrying AC current from a step-down isolation transformer, heating it to 150-250 C.

E. First Ion Funnel

After emerging from the transfer capillary, the ions enter an ion funnel, based on the design of Smith and coworkers,[32] consisting of 50 nickel-plated brass electrodes, each 1mm thick and separated by 1mm thick PTFE washers. Each electrode has a circular opening, the first 10 of which are 34 mm diameter. Thereafter, the diameter decreases linearly to 3 mm. The first and last electrodes have only DC potentials applied to them, whereas the potentials of the intervening electrodes are a superposition of a radio frequency (RF) potential, with opposite phases applied to alternating electrodes, and a DC potential that is set by a voltage divider along the length. The RF field confines the ions radially as they are driven through the funnel by the DC potential gradient. The RF potential for the funnel (f=500 kHz) is generated by a dedicated power supply the output of which is capacitively coupled to the ion funnel and is capable of supplying up to 720 V_{pp} (although electrical breakdown of the gas typically occurs at much lower amplitudes). The DC potentials to the electrodes are set by a resistive voltage divider, with the total potential drop across the funnel normally being 180 V. The aperture of the final electrode of the ion funnel is covered by fine Ni mesh, and can be switched by up to 65 V with respect to the adjacent electrodes. This allows it to act as an ion gate; ions accumulate in the funnel when the gate potential is high, and are released when the potential is dropped. The gate is normally triggered at 20 Hz with an opening time of 50-500 μs.

F. Drift Region

The electric field in the drift region is sustained by 82 stainless steel electrodes (1 mm thick, laser cut) with 34 mm apertures. These electrodes are mounted into slots in a PMMA bed, which, if necessary, can be removed from the main PMMA housing. The drift electrodes are arranged so that a 38.5 cm long straight section is preceded and followed by two S-bends (see Figs. 1 &2). Appropriately positioned holes (9 mm diameter) cut into the S-bend electrodes allow a laser beam to coaxially overlap ions travelling through the straight section of the drift tube. The first 5 electrodes (immediately following the ion funnel) have 5 mm diameter openings and are separated by 5 mm. The remaining electrodes have 34 mm openings, and are 12 mm apart. The electrodes are connected in series by 1 MΩ resistors to make a voltage divider such that the electrode potentials are provided by a single high voltage power supply.

Halfway along the drift region is a second ion gate that can be opened briefly to select a packet of isomers that have separated from other isomers in the first part of the drift region. The gate, based on the design of Bradbury and Nielsen,[33] consists of two 0.1 mm

Nichrome wires loomed on a 3D-printed RGD840 polymer former, such that in the central region the wires alternate and are spaced by 0.6 mm. To block ions the potential of one wire is raised by 18 V with respect to the other, whereas to pass ions the wires are set to the same potential.

A crucial feature of the instrument is provision for a tunable laser beam to overlap the ion bunch, modifying their isomeric form, and hence alter their drift mobilities. Provision has been made for both coaxial and transverse excitation of the drifting ions. The machine was designed so that the drifting ions could be overlapped coaxially with the output beam of a continuous laser, necessitating introduction of two S-bend sections into the drift region (see Fig. 1). Although curved drift sections have been employed in other ion mobility spectrometers,[34] they have normally been followed by an ion funnel to regather the ions to the centre of the drift tube. Modelling of the S-bend sections using ion optics simulation software (SIMION 3D v8.0.5) and a statistical diffusion simulation program,[35,36] shows that as the ion bunch moves around the first curve, ions on the inside move ahead of ions on the outside, due to the shorter path length and higher electric field (see Figure 3). This longitudinal spreading is countered in the second part of the curve where ions with a shorter path in the first curve have a longer path and vice versa, although because the ion packet has spread radially there is some overcompensation.

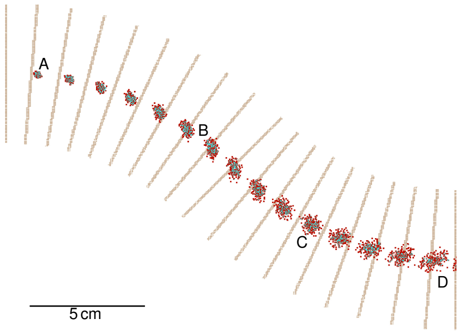

FIG. 3. Simulation of 200 Da ions drifting through 15 Torr of N_2 propelled by an electric field that is 50 V/cm along the centreline. Ion packet snapshots are shown for 400 μs time intervals. The initial spherical ion packet (A) is distorted as it traverses the first bend with ions on the inside moving ahead of ions on the outside (B). The deformation is corrected in the second bend (C), although the ion packet still ends up being slightly distorted (D). Simulation details are given in the text.

G. Second Ion Funnel

The drift region ends with a second ion funnel, consisting of 40 electrodes with the aperture diameter decreasing linearly, from 34 mm to 3 mm, which operates with an RF drive frequency of 500 kHz. The funnel is followed by a 1 mm thick stainless steel plate with a 0.35 mm orifice leading into a differentially pumped section containing an octopole ion guide, which confines the ions radially, while allowing neutral gas to be evacuated. The ions then pass through another orifice (3 mm diameter) into a final chamber, containing a lens stack that focuses the ions into the quadrupole mass filter (Extrel C50, 19 mm rods, f=1.2 MHz).

H. Ion Detection, Signal Processing and Equipment Control

The ions are detected by an electron multiplier (Photonis Channeltron 4870E) operating in single ion counting mode. The output of the detector is sent to a pulse amplifier/discriminator (MIT Inc. Model F-100T), the TTL output of which is passed to a multichannel scaler (FAST ComTec P7882, bin width 10 μs) that logs each pulse in one of two histograms (one for laser-on arrivals and the other for laser-off arrivals), to progressively collect laser-on and laser-off arrival time distributions (ATDs); the difference between the two ATDs reflects the change resulting from exposing the ions to laser light. Synchronization of the two ion gates and the pulsed laser is accomplished using digital delay generators (Stanford Research Systems Model DG535 and Berkerley Nucleonics Corporation Model 575). The instrument is controlled by a Labview (National Instruments) Virtual Instrument (VI), that sets the quadrupole mass filter and OPO wavelength, and reads the arrival time distribution data from the multichannel scaler.

I. Photoexcitation

The light source for most investigations has been a pulsed optical parametric oscillator with a scan range of 220-2500 nm (5 cm^{-1} bandwidth, 5 ns pulse width).[23–25] Normally, ions are injected into the drift region at 20 Hz with the laser fired at 10 Hz so that laser-on and laser-off ATDs are recorded. The photo-signal corresponds to the difference between laser-on and laser-off ATDs. Photoisomerization has also been accomplished using the output of a quasi-continuous Titanium:Sapphire laser with mechanical chopping of the light beam to record laser-on and laser-off ATDs and discern the laser-induced signal.[23]

As shown in Figure 1, the drifting ions can either be excited at the beginning of the drift region (Mode 1), after a second ion gate halfway along the drift region (Mode 2), or coaxially in the central part of the drift region (Mode 3). The three excitation modes are described in more detail below.

Mode 1:

Ions are irradiated 30-40 mm after the first ion gate by a transverse burst of light from a pulsed laser. Parent, photo-isomer and photofragment ions are spatially and temporally separated after passage through the drift tube. The advantage of this operational mode is that the entire ion packet, which at this stage has a diameter of ≈3 mm, can be irradiated with a relatively intense laser beam before appreciable diffusional spreading. A drawback is that one measures the net effect of laser excitation. For example, if the ion packet contains 2 isomers (I_1 and I_2), then the laser beam potentially causes $I_1 \rightarrow I_2$ and $I_2 \rightarrow I_1$ photoisomerizations with the I_1 and I_2 photo-isomer ions arriving at practically the same time as ions produced directly by the ion source. Therefore, any photo-isomerization signal is observed against a background.

Mode 2:

Packets of ions are irradiated halfway along the drift region after being mobility-selected by the second ion gate. For this mode, the second ion gate is opened for ≈100 μs at an appropriate delay after opening the first gate to transmit a packet of the desired target ions. A short time later a transverse laser pulse intercepts the selected ions ≈15 mm downstream from the ion gate. Mode 2 has the considerable advantage that a packet of mobility-selected isomers is excited with spatial and temporal separation of the photo-isomers over the remainder of the drift region. Consequently, the photo-isomer signal can often be observed against a zero background. Normally, the laser beam is expanded to have a relatively large cross section (≈4 mm×10 mm) to ensure that the entire ion packet is exposed to light. This IMS-photoexcitation-IMS-MS arrangement is analogous to the IMS-collision-IMS-MS approach of Clemmer and co-workers, where ions selected by the first IMS stage are subjected to a collisional excitation in a region with enhanced electric field strength with separation of the collisionally produced isomers in a second IMS stage.[12]

Mode 3:

The ions are irradiated coaxially in the straight section of the drift region by the beam from a pulsed or continuous laser passing through holes cut into the S-bend drift electrodes. This excitation mode was employed in our original investigations of the carbocyanine dye HITC,[23] using light from a continuous Ti-Sapphire laser (λ=740-860 nm, intensity $\sim$1 W/cm^2) chopped with a mechanical shutter to record laser-on and laser-off arrival time distributions (ATDs). Mode 3 is potentially useful for molecular ions that are optically pumped from the ground state to an excited state, and which rapidly relax to the ground state. Under these circumstances, laser excitation can potentially be used to establish a light-driven equilibrium between the ground and excited states, which, assuming the ground and excited state ions have different drift mobilities, should induce a change in the ions' arrival time distribution.

Although, our photoisomerization studies have mainly employed Mode 1 or Mode 3,[23–26] as explained below in Section IV B there are significant advantages in using Mode 2, with preselection of the target isomers based on their mobilities. Future studies are likely to use this approach.

One disadvantage of the current IMMS machine is that laser light with wavelengths shorter than 310 nm tends to produce background ions in the drift tube region, presumably through multiphoton ionization of organic contaminants. Background ionisation is not a problem for light with $\lambda \geq$310 nm.

IV. INSTRUMENT PERFORMANCE

In the following section we summarise the performance of the IMMS instrument and present examples of its use to characterise the photoisomerization and photodissociation of molecular ions.

A. IMMS Performance

With the first and second ion gates fully open, the ion count rate for electrosprayed tetrabutylammonium (TBA) cations (m/z=242 Da) is $\approx 10^6$ s^{-1}, dropping to 5×10^3 s^{-1} if the first ion gate is pulsed at 20 Hz with 100 μs opening time (with the second ion gate

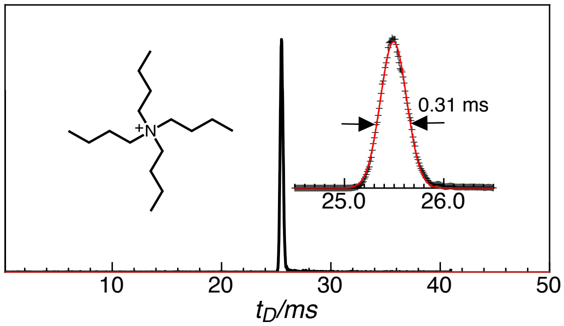

FIG. 4. Arrival time distribution (ATD) for electrosprayed TBA ions propelled through 10.8 Torr of N_2 gas. Inset is an expanded view of the peak fitted by a Gaussian function. The peak width corresponds to a mobility resolution of 82.

open). The instrument has an effective mass range of 100-440 amu with the lower limit determined by the 500 kHz drive frequency for the ion funnels, and upper limit by the quadrupole mass filter.

An important measure for an ion mobility spectrometer's performance is the resolving power. which for an ideal drift tube IMS instrument, R, is given by,[27]

$$R = \frac{t_d}{\Delta t} = \left[\frac{16\, kT\, ln2}{Vze} + \left(\frac{\Delta t_0}{t_d} \right)^2 \right]^{-1/2} \tag{4}$$

where, t_d is the drift time, Δt is the width of the detected pulse, V is the potential drop across the drift region, and Δt_0 is the temporal width of the ion packet at launch (presumed to have a Gaussian profile).[27] The first term in Eqn. 4 corresponds to diffusional spreading of the ion packet whereas the second term accounts for the finite temporal width of the injected ion pulse. The instrument's performance is illustrated in Fig. 4, which shows an arrival time distribution (ATD) for tetrabutylammonium cations with a potential drop of 4.57 kV across the drift region and a gate opening time of 100μs, demonstrating a mobility resolution of 82. This compares with a diffusion limited resolution of 101 predicted using Eqn. 4 and taking into account the ions' passage through the drift region and the second ion funnel (where the drift field is lower). The instrument routinely achieves a mobility resolution of 75-85 for singly charged ions. Employing the second electrostatic gate halfway along the drift region gives the machine an IMS-IMS capacity (Mode 2, see Fig. 1), with each stage having a mobility resolution of ≈50 for singly charged ions.

B. Photoisomerization of Molecular Ions

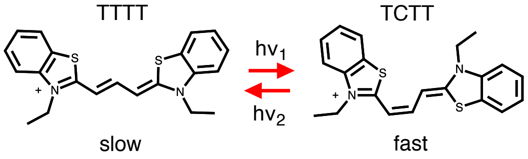

FIG. 5. Photoisomerization of DTC$^+$ molecules.

The machine's capacity to probe photoisomerization of molecular ions is conveniently illustrated for carbocyanine dyes, which consist of a polymethine chain terminated at each end by an aromatic group (Fig. 5). Carbocyanines, which have been extensively studied in solution,[37–40] absorb light strongly in the visible region, with photo-excitation causing *trans*-*cis* photoisomerization about one of the C-C bonds in the polymethine chain. Specifically, we consider the carbocyanine molecule DTC$^+$, comprising two aromatic groups linked by a conjugated chain of 3 carbon atoms. Each of the C-C bonds can have either a *trans* (T) or *cis* (C) conformation, giving 10 distinguishable isomers (TTTT, CTTT, TCTT, CCTT, CTCT, CTTC, TCCT, CCCT, CTCC, CCCC). The ATD collected for an electrosprayed DTC$^+$ sample, with no laser radiation and with the second ion gate opened to pass all ions [Fig. 6(a)], displays clear evidence for two isomers with arrival times of t_D=26.2 and 25.6 ms. The two peaks can be assigned as the TTTT and TCTT isomers on the basis of density functional theory (DFT) calculations and computed drift mobilities (based classical trajectory calculations using the DFT equilibrium geometries).[24] The TTTT and TCTT isomers lie lowest in energy (relative energies of 0 and 13.7 kJ/mol) and are expected to dominate the drifting ion population, with the more compact TCTT isomer having a 2.5% higher mobility than the extended TTTT isomer.[24]

By opening the second ion gate for 100 μs at an appropriate delay with respect to the first gate, either the TTTT or TCTT isomer can be selected [Figures 6(b) and (c)]. Photoexcitation of the mobility-selected TTTT or TCTT isomers with a laser pulse (λ=532 nm, I=1-2 mJ/pulse/cm^2) immediately after the second gate causes photoisomerization - TTTT isomers are transformed to TCTT isomers and vice versa. In both cases, the depletion of one isomer is balanced to within 1% by formation of the other isomer, proving that photofragmentation and other loss mechanisms are negligible. The data presented in Figure 6 show that by using the second ion gate one can cleanly separate and irradiate

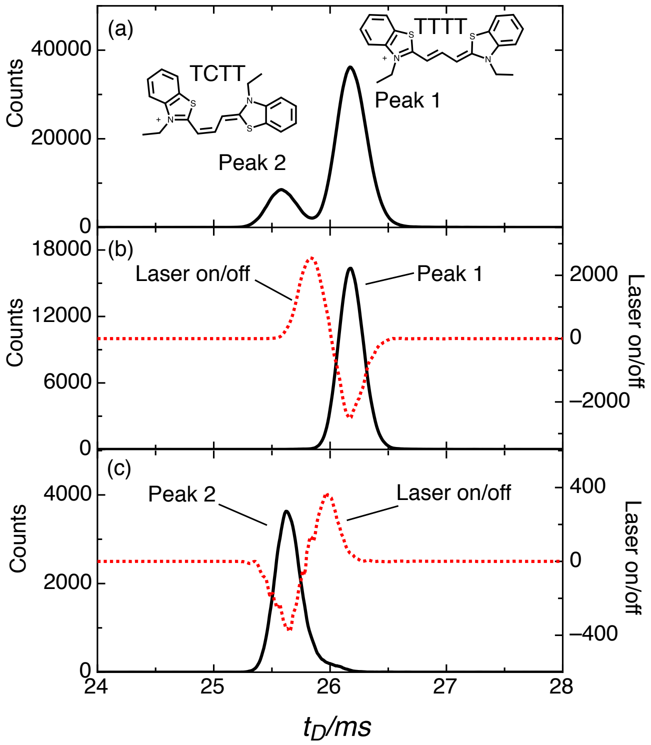

FIG. 6. (a) Laser-off ATD for DTC$^+$ with second ion gate open. The two peaks correspond to the TTTT and TCTT isomers. (b) ATD with second ion gate selecting TTTT DTC$^+$(Peak 1). The red dotted trace shows the laser on-laser off signal at λ=532 nm, which causes TTTT→TCTT isomerization. (c) ATD with second ion gate selecting TCTT DTC$^+$(Peak 2). Radiation at 532 nm causes TCTT→TTTT isomerization.

isomers whose collision cross sections differ by 2%.

Through measuring the photo-isomer signal as a function of the laser wavelength, it is possible to obtain a photoisomerization action (PISA) spectrum corresponding to the molecule's absorption spectrum [$A(\lambda)$] convoluted with the photoisomerization yield [$\phi(\lambda)$]. As shown in Fig. 7(b), the PISA spectra for the two isomers are different; the spectrum for the TTTT isomer has a peak ≈10 nm to longer wavelength than that for the TCTT isomer. This is consistent with spectra for DTC$^+$ in methanol solution [Figure 7(c)], where the absorption spectrum for all-*trans* DTC$^+$ has a peak 10 nm to longer wavelength than that of the photo-isomer. Also noteworthy is that the bands for DTC$^+$ in solution are shifted 25 nm to longer wavelength compared to the maxima of the gas-phase spectra. The similarity with the solution spectra suggests that the PISA spectra of the TTTT and TCTT isomers actually mimic their absorption spectra and that in this case the isomerization yield $\phi(\lambda)$ is independent of wavelength. Previously, we have modelled the DTC$^+$ photoisomerization as a process in which the electronically excited molecules undergo internal conversion to the electronic ground state followed by isomerization, with stabilisation of the vibrationally energised isomers through collisional quenching by buffer gas molecules.[24] Under these circumstances, because the photon energy (200-260 kJ/mol) is much larger than the isomerization barriers (40-90 kJ/mol), one would expect that the isomerization yield should be almost independent of wavelength.

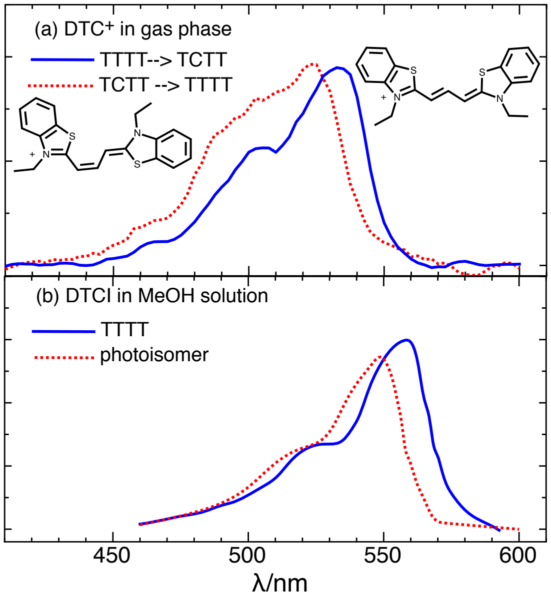

FIG. 7. (a) PISA spectra for isomers of DTC$^+$, showing wavelength dependence for the TTTT→TCTT isomerization (solid blue curve) and TCTT→TTTT isomerization (dashed red curve). (b) Absorption spectra of all-*trans* DTC$^+$ and DTC$^+$ photoisomer in methanol solution.[37,41]

C. Photodissociation of Molecular Ions

At higher laser intensities molecular ions in the drift region undergo resonance enhanced photofragmentation so that the apparatus can also be used to measure photofragmentation action spectra. Although photodissociation studies of molecular ions are conveniently conducted using tandem mass spectrometers or ion traps, with many different arrangements already described in the literature,[16,18,22,42,43] the IMMS device has the advantage that structural information for the fragment ions can be derived from their

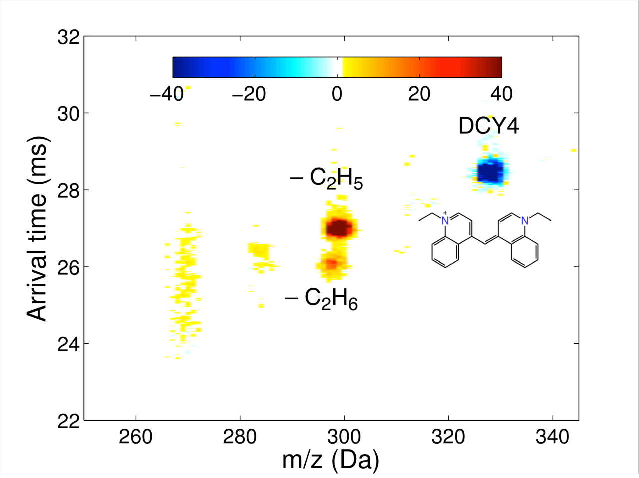

FIG. 8. Photofragment signal from DCY4$^+$ as a function of mass and arrival time with OPO wavelength set to 570 nm. Laser induced depletion of the DCY4 ions at 328 Da is matched by enhancement of ions corresponding to loss of C_2H_5 and C_2H_6.

collision cross sections. We have exploited this feature to deduce that the m/z=248 Da photofragment from the retinal protonated Schiff base is the protonated Schiff base of β-ionone rather than a previously postulated bicyclic structure.[26,44]

As an example of the IMMS machine's capacity for photodissociation spectroscopy, Fig. 8 plots the photo-signal for the polymethine dye 1,1′-diethyl-4,4′-cyanine (DCY4$^+$) as a function of arrival time and mass, with the ions irradiated at the beginning of the drift tube (Mode 1) with light at a wavelength of 570 nm (I ≈10 mJ/pulse/cm^2). Depletion of the parent DCY4$^+$ ions (m/z=327 Da, t_d= 28.3 ms) is accompanied by production of fragments with masses of 298, 297, 267, 268, 269 Da, corresponding to loss of one or two ethyl radicals or ethane molecules from the terminal aromatic heterocycles. The lower panel of Fig. 9 shows the difference between the laser-off and laser-on ion signals as a function of arrival time and laser wavelength for DCY4$^+$ and photofragments. Here, the second quadrupole is run in RF-only mode to transmit all ions. Photofragments arriving at 27 and 26 ms correspond to DCY4$^+$ cations that have shed an ethyl radical or ethane molecule, respectively. The resonance enhanced photodissociation spectrum for DCY4$^+$, obtained by plotting the photofragment yield as a function of wavelength, overlaps the absorption band of DCY4$^+$ in aqueous solution (Fig. 9, upper panel), showing that in this case there is minimal shift in the absorption band caused by the solvent.

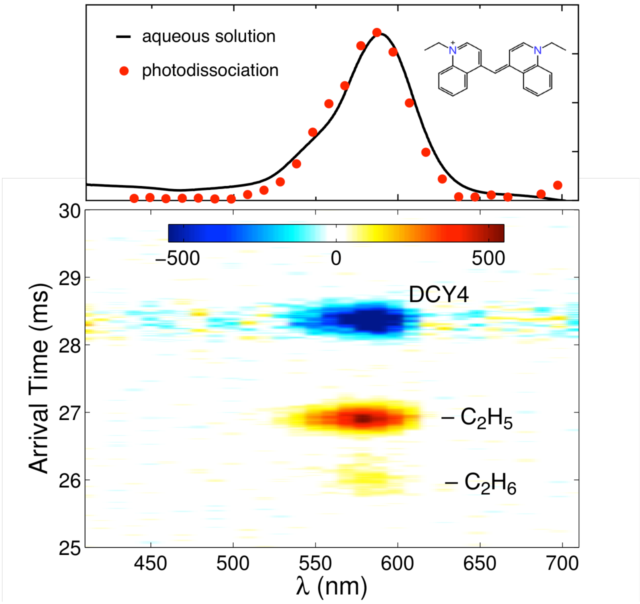

FIG. 9. Lower panel: Photofragment signal for DCY4$^+$ cations as a function of wavelength and arrival time. The quadrupole mass filter was operated in RF-only mode to transmit all ions. Upper panel: Resonance enhanced photodissociation action spectrum of DCY4$^+$ cations recorded by plotting the –C_2H_5 photofragment signal as a function of laser wavelength.

V. SUMMARY AND OUTLOOK

The IMMS apparatus provides a new means for investigating photoisomerization of molecular ions in the gas phase, with the advantages of isomer selection prior to the spectroscopy stage and identification of the product isomer(s). The apparatus can also be used for photodissociation studies, with the advantage that the charged product's can be identified from both its drift mobility and mass. Although most previous studies have involved photo-exciting molecular ions at the beginning of the drift tube (Mode 1),[23–26] there are significant advantages in separating the target isomer before irradiation (Mode 2). There are numerous molecular ions suitable for the new approach, including systems that are important in biology (protein chromophores, retinal, carotenoids) or in light-activated devices (spiropyrans, diarylethenes, fulgides, azobenzenes). The main drawback of the approach for obtaining spectra of molecular ions is that it is only suitable for species that photoisomerize. Although this may seem like a severe restriction limiting the technique to larger molecules, in fact many small charged molecules have several isomeric forms.

For example, even a small molecular ion like $C_3H_3^+$ exists as both the cyclopropenyl and propargyl cations which will have significantly different collision cross sections and which may be interconvertible through photo excitation.

ACKNOWLEDGMENTS

Construction of the IMS apparatus was possible because of outstanding technical input from R. Mathys, Science Faculty Workshop. This research was supported under the Australian Research Council's Discovery Project funding scheme (Project Numbers DP110100312 and DP120100100).

REFERENCES

[1] B. L. Feringa, *Molecular Switches*, edited by B. L. Feringa and W. R. Browne, Vol. 1 (Wiley-VCH, Weinheim, 2001).

[2] W. Browne and B. Feringa, Annu. Rev. Phys. Chem. **60**, 407 (2009).

[3] J. Conyard, K. Addison, I. A. Heisler, A. Cnossen, W. R. Browne, B. L. Feringa, and S. R. Meech, Nature Chem. **4**, 547 (2012).

[4] G. von Helden, M. Hsu, N. Gotts, and M. Bowers, J. Phys. Chem. **97**, 8182 (1993).

[5] R. R. Hudgins, M. Imai, M. F. Jarrold, and P. Dugourd, J. Chem. Phys. **111**, 7865 (1999).

[6] P. R. Kemper, N. F. Dupuis, and M. T. Bowers, Int. J. Mass Spectrom. **287**, 46 (2009).

[7] F. Lanucara, S. W. Holman, C. J. Gray, and C. E. Eyers, Nature Chem. **6**, 281 (2014).

[8] A. B. Kanu, P. Dwivedi, M. Tam, L. Matz, and H. H. Hill Jr, J. Mass Spec. **43**, 1 (2008).

[9] N. A. Pierson, L. Chen, D. H. Russell, and D. E. Clemmer, J. Am. Chem. Soc. **135**, 3186 (2013).

[10] T. Wyttenbach, N. A. Pierson, D. E. Clemmer, and M. T. Bowers, Ann. Rev. Phys. Chem. **65**, 175 (2014).

[11] K. Ohshimo, T. Komukai, R. Moriyama, and F. Misaizu, J. Phys. Chem. A **118**, 3899 (2014).

[12] N. A. Pierson and D. E. Clemmer, Int. J. Mass Spectrom. **in press**, DOI: 10.1016/j.ijms.2014.07.012 (2014).

[13] P. R. Kemper and M. T. Bowers, Journal of the American Society for Mass Spectrometry **1**, 197 (1990).

[14] M. Kohtani, J. E. Schneider, T. C. Jones, and M. F. Jarrold, J. Am. Chem. Soc. **126**, 16981 (2004).

[15] D. Polli, P. Altoè, O. Weingart, K. M. Spillane, C. Manzoni, D. Brida, G. Tomasello, G. Orlandi, P. Kukura, R. A. Mathies, M. Garavelli, and G. Cerullo, Nature **467**, 440 (2010).

[16] M. A. Duncan, Int. J. Mass Spectrom. **200**, 545 (2000).

[17] E. J. Bieske and O. Dopfer, Chem. Revs. **100**, 3963 (2000).

[18] R. C. Dunbar, Int. J. Mass Spectrom. **in press**, DOI: 10.1016/j.ijms.2014.07.049 (2014).

[19] K. Muller-Dethlefs and E. W. Schlag, Ann. Rev. Phys. Chem. **42**, 109 (1991).

[20] L. Zhu and P. Johnson, J. Chem. Phys. **94**, 5769 (1991).

[21] R. N. Zare, Annu. Rev. Anal. Chem. **5**, 1 (2012).

[22] T. R. Rizzo, J. A. Stearns, and O. V. Boyarkin, Int. Rev. Phys. Chem. **28**, 481 (2009).

[23] B. D. Adamson, N. J. A. Coughlan, R. Continetti, and E. J. Bieske, Phys. Chem. Chem. Phys. **15**, 9540 (2013).

[24] B. D. Adamson, N. J. A. Coughlan, G. da Silva, and E. J. Bieske, J. Phys. Chem. A **117**, 13319 (2013).

[25] N. J. A. Coughlan, K. J. Catani, B. D. Adamson, U. Wille, and E. J. Bieske, J. Chem. Phys. **140**, 164307 (2014).

[26] N. J. A. Coughlan, B. D. Adamson, K. J. Catani, U. Wille, and E. J. Bieske, J. Phys. Chem. Lett. **5**, 3195 (2014).

[27] H. E. Revercomb and E. A. Mason, Anal. Chem. **47**, 970 (1975).

[28] E. W. Mason, E. A.; McDaniel, *Transport Properties of Ions in Gases* (John Wiley, New York, 1988).

[29] A. A. Shvartsburg and M. F. Jarrold, Chem. Phys. Letts. **261**, 86 (1996).

[30] M. Mesleh, J. Hunter, A. Shvartsburg, G. Schatz, and M. Jarrold, J. Phys. Chem. **100**, 16082 (1996).

[31] M. F. Mesleh, J. M. Hunter, A. A. Shvartsburg, G. C. Schatz, and M. F. Jarrold, J. Phys. Chem. A **101**, 968 (1997).

[32] R. T. Kelly, A. V. Tolmachev, J. S. Page, K. Tang, and R. D. Smith, Mass Spectrom. Rev. **29**, 294 (2009).

[33]N. Bradbury and R. Nielsen, Phys. Rev. **49**, 388 (1936).

[34]S. I. Merenbloom, R. S. Glaskin, Z. B. Henson, and D. E. Clemmer, Anal. Chem. **81**, 1482 (2009).

[35]A. Appelhans and D. Dahl, Int. J. Mass Spectrom. **244**, 1 (2005).

[36]H. Lai, T. McJunkin, C. Miller, J. Scott, and J. Almirall, Int. J. Mass Spectrom. **276**, 1 (2008).

[37]G. Ponterini and F. Momicchioli, Chem. Phys. **151**, 111 (1991).

[38]I. Baraldi, A. Carnevali, F. Momicchioli, and G. Ponterini, Spectrochim. Acta, Part A **49A**, 471 (1993).

[39]M. Krieg and R. W. Redmond, Photochem. Photobiol. **57**, 472 (1993).

[40]P. F. Aramendia, R. M. Negri, and E. S. Roman, J. Phys. Chem. **98**, 3165 (1994).

[41]R. E. Di Paolo, L. B. Scaffardi, R. Duchowicz, and G. M. Bilmes, J. Phys. Chem. **99**, 13796 (1995).

[42]D. C. McGilvery and J. D. Morrison, J. Chem. Phys. **67**, 368 (1977).

[43]A. Dzhonson, D. Gerlich, E. J. Bieske, and J. P. Maier, J. Mol. Struct. **795**, 93 (2006).

[44]Y. Toker, D. B. Rahbek, H. V. Kiefer, J. Rajput, R. Antoine, P. Dugourd, S. B. Nielsen, A. V. Bochenkova, and L. H. Andersen, Phys. Chem. Chem. Phys. **15**, 19566 (2013).